Short Communication:

Synthesis, Characterization, and Bioactivity Evaluation of V(IV), Fe(III), Cr(III), Mn(II), Mo(VI), and Ru(III) Complexes with a New Azo Dye Ligand

Ban Hasan Ali Al-Agele and Areej Kamal Assim Al-Dabbagh*

Department of Chemistry, College of Science for Women, University of Baghdad, Al-Jadriya Street, Baghdad 10071, Iraq

* ***Corresponding author:***

tel: +964-7811133481
email: areej.k@csw.uobaghdad.edu.iq

Received: August 21, 2025
Accepted: November 10, 2025

DOI: 10.22146/ijc.110564

Abstract: *The new azo dye ligand 1-(2,4,6-trihydroxy-3-(2-hydroxy-phenylazo)phenyl)ethanone (H_2L) was produced by reacting the diazonium salt derived from 2-aminophenol, with 2,4,6-trihydroxyacetophenone. This ligand was used to create several azo dye-metal complexes through reactions with salts of V(IV), Fe(III), Cr(III), Mn(II), Mo(VI), and Ru(III). The ligand was characterized using ^{1}H- and ^{13}C-NMR spectroscopy. The metal complexes were analyzed via UV-vis, FTIR, MS, thermal analysis (TGA, DSC), conductivity measurements, magnetic susceptibility, metal/chlorine content, and melting point determination. The results showed that the ligand acts as a tetradentate ligand with Ru, Mo, and VO, and as a tridentate ligand with Cr, Mn, and Fe. All complexes were octahedral in shape, except for the vanadium complex, which exhibited a square pyramidal structure. All complexes exhibited non-electrolytic properties. The compounds' capacity to act as antioxidants was assessed by measuring their ability to inhibit the DPPH free radical, with ascorbic acid serving as a standard reference. The half-maximal inhibitory concentration (IC_{50}) values were determined, revealing the following order of activity: H_2L > Ru-complex > Fe-complex > ascorbic acid = VO-complex = Mo-complex > Mn-complex > Cr-complex. The compounds were also tested for antibacterial and antifungal activity at two concentrations.*

Keywords: *antioxidant capacity; azo dye-complexes; biological activity; conductivity; diazonium salt*

■ INTRODUCTION

The term "azo" originates from the French word "azoate", which has long been associated with nitrogen. Azo dyes, the most common class of organic compounds, have attracted the interest of numerous researchers due to their significance and widespread use in various industries, particularly textiles, paper, and plastics. These dye compounds are characterized by their bright and diverse colors, resulting from the presence of the azo (–N=N–) functional group [1], which connects two aromatic rings in their molecular structure [2]. They are produced by reacting aromatic amines with specific oxidizing agents, resulting in dyes with excellent chemical and light stability, as well as distinct color properties [3]. Some azo derivatives are used in pharmaceuticals, leather, and polymer industries. In contrast, others are employed in the production of fabric, plastic, and ink due to their broad spectrum of colors and good stability [4-5]. Coordination chemistry heavily involves second-row transition metals such as molybdenum (Mo) and ruthenium (Ru), which can form stable complexes with azo ligands and act as anticancer agents due to their role in long-wavelength photodynamic therapy. Through electron donation and back-donation interactions, the partially filled *d*-orbitals of these metals enable the formation of strong coordination bonds with azo ligands.

Additional stability across different metal ion oxidation states arises from the acidic characteristics of the π-orbitals in nitrogen-heterocycles involved in azo units, particularly in acid dye-Cr(III) complexes that have numerous applications in skin and hair coloring.

Azo-metal complexes are considered novel, cost-effective compounds with a range of anti-inflammatory, antibacterial, and anticancer properties, owing to their interactions with proteins and other macromolecules, such as DNA [6-8]. Such combinations are vital for drug development, especially for metal-based anticancer drugs [9-11], and antioxidants [12]—both natural and synthetic—that can neutralize free radicals through mechanisms such as capture, repair, and avoidance, which are fundamental for boosting immunity [13]. Furthermore, these complexes have garnered extensive research interest due to their unique chemical and physical properties, including excellent thermal stability, catalytic activity, and UV-visible light absorption capabilities. Due to these qualities, they have applications in the fields of medical research, environmental remediation, and organic catalysis [14-16]. This work aims to synthesize a new azo ligand, 1-(2,4,6-trihydroxy-3-(2-hydroxy-phenylazo)phenyl)ethanone (H_2L), by reacting 2-aminophenol (which contains ortho-amino and hydroxyl groups that aid in heterocycle formation) with 2,4,6-trihydroxyacetophenone (a starting compound with polar and UV-absorbing properties). The ligand will be used to coordinate with metal ions, such as V(IV), Fe(III), Cr(III), Mn(II), Mo(VI), and Ru(III), forming complexes. The stability and thermal decomposition of these complexes were analyzed using spectroscopy, DSC, TGA curves, and melting points. The complexes exhibited notable chemical and physical characteristics, such as high thermal stability and UV-visible light absorption, confirmed through ^{1}H- and ^{13}C-NMR, conductivity, magnetic susceptibility, and C.H.N. analysis. Additionally, antibacterial and antifungal activities of the azo ligand and its metal complexes were evaluated. The antioxidant activity of the ligand complexed with V(IV), Fe(III), Cr(III), Mn(II), Mo(VI), and Ru(III)was also assessed against the DPPH radical, using ascorbic acid as a reference natural antioxidant.

■ EXPERIMENTAL SECTION

Materials

All components, chemicals, and reagents were obtained from commercial suppliers (Sigma-Aldrich, Merck). The materials included 2-aminophenol (98%), 2,4,6-trihydroxyacetophenone (98.5%), NaOH (98%), $VOSO_4{\cdot}5H_2O$ (99.8%), $MnCl_2{\cdot}4H_2O$ (96%), $CrCl_3{\cdot}6H_2O$ (99%), $FeCl_3$ (98%), $RuCl_3{\cdot}3H_2O$ (98%), and $(NH_4)_2MoO_4$ (99%), as well as $NaNO_2$ (98%). Solvent media consisted of absolute ethanol (99.8%), concentrated HCl (99.8%), and 96% DMSO.

Instrumentation

Measurements of the prepared compounds were carried out using the elemental microanalysis technique (C.H.N.), performed with the Urovector model EA/3000, singleV3O, to ensure compound purity by comparing the practical ratio with the theoretical ratio. The AAS device was used to determine the metal's mass percentage. The ions were identified as M–O through gravimetric methods. Molar conductivity was measured using a conductivity meter (W-T-W) at 25 °C with a 1×10^{-3} M solution. UV-vis absorption spectra were recorded with a Shimadzu UV-1800 spectrophotometer. ^{1}H- and ^{13}C-NMR spectra were obtained using a Bruker (400 MHz) spectrometer. Fourier-transform infrared (FTIR) spectra were acquired using an IR Prestige-21, with instruments including Bruker 4,000–400 cm^{-1} and Shimadzu 4,000–200 cm^{-1}. The metal contents were identified using a Shimadzu (F.A.A) 680 G atomic absorption device. Magnetic properties were analyzed with the equilibrium magnetic susceptibility model, MSR-MKI. All other thermal analyses were performed using a Perkin-Elmer Pyris Diamond DSC/TGA.

Procedure

Synthesis of azo dye ligand

In this study, 1-(2,4,6-trihydroxy-3-(2-hydroxy-phenylazo)phenyl)ethanone was prepared through a diazotization–coupling reaction. Typically, 1.0 g (9.160 mmol) of 2-aminophenol was dissolved in a mixture of 15 mL of ethanol and 10 mL of distilled water. To this, 3 mL of conc. HCl and 0.632 g (9.15 mmol) of $NaNO_2$ (previously dissolved in distilled water) were added. The mixture was stirred vigorously for 45 min to form the diazonium salt. Next, 1.328 g (9.160 mmol) of 2,4,6-trihydroxyacetophenone, dissolved in 20 mL of ethanol, was added to the reaction mixture and stirred

thoroughly for an additional 30 min. The resulting reddish-brown suspension was filtered and dried at room temperature for 24 h. This procedure produced the desired compound with an estimated yield of 78%.

General approach for metal complexes synthesis

The azo dye ligand (H_2L) 1.0 g (0.003 mmol) was dissolved in 15 mL of hot ethanol. Into the ligand solution, 0.3 g (0.007 mmol) of NaOH (previously dissolved in distilled water) was added. After 10 min of vigorous stirring, the metal ion (0.003 mmol) was added, which could be one of the following: 0.1 g $VOSO_4{\cdot}5H_2O$, 0.6 g $FeCl_3$, 0.7 g $(NH_3)_2MoO_4$, 0.9 g $RuCl_3{\cdot}3H_2O$, 0.7 g $MnCl_2{\cdot}4H_2O$, or 1 g $CrCl_2{\cdot}6H_2O$, all dissolved in 15 mL of distilled water, while $RuCl_3{\cdot}3H_2O$ was dissolved in 15 mL of water with the addition of three drops of HCl. Subsequently, the solutions were subjected to reverse osmosis for 7 h at 40 °C. Afterward, the reaction mixtures were heated and purified while still hot. The resulting precipitate was collected, rinsed with a 1:1 water-ethanol mixture, and dried at room temperature for 24 h. This procedure yielded the desired products with an approximate yield ranging from 73 to 88%. Scheme 1 illustrates the synthesis steps, from ligand preparation to the formation of metal complexes.

Biological activity

The bacterial test was prepared with two concentrations, 1 and 500 M, of the ligand and its complexes in 1 mL of DMSO solvent, and tested against two types of pathogenic bacteria: *Bacillus* spp. ATCC 6051 (Gram-positive) and *Escherichia coli* ATCC 25922 (Gram-negative). The test employed a method such as agar diffusion, where effectiveness is observed through

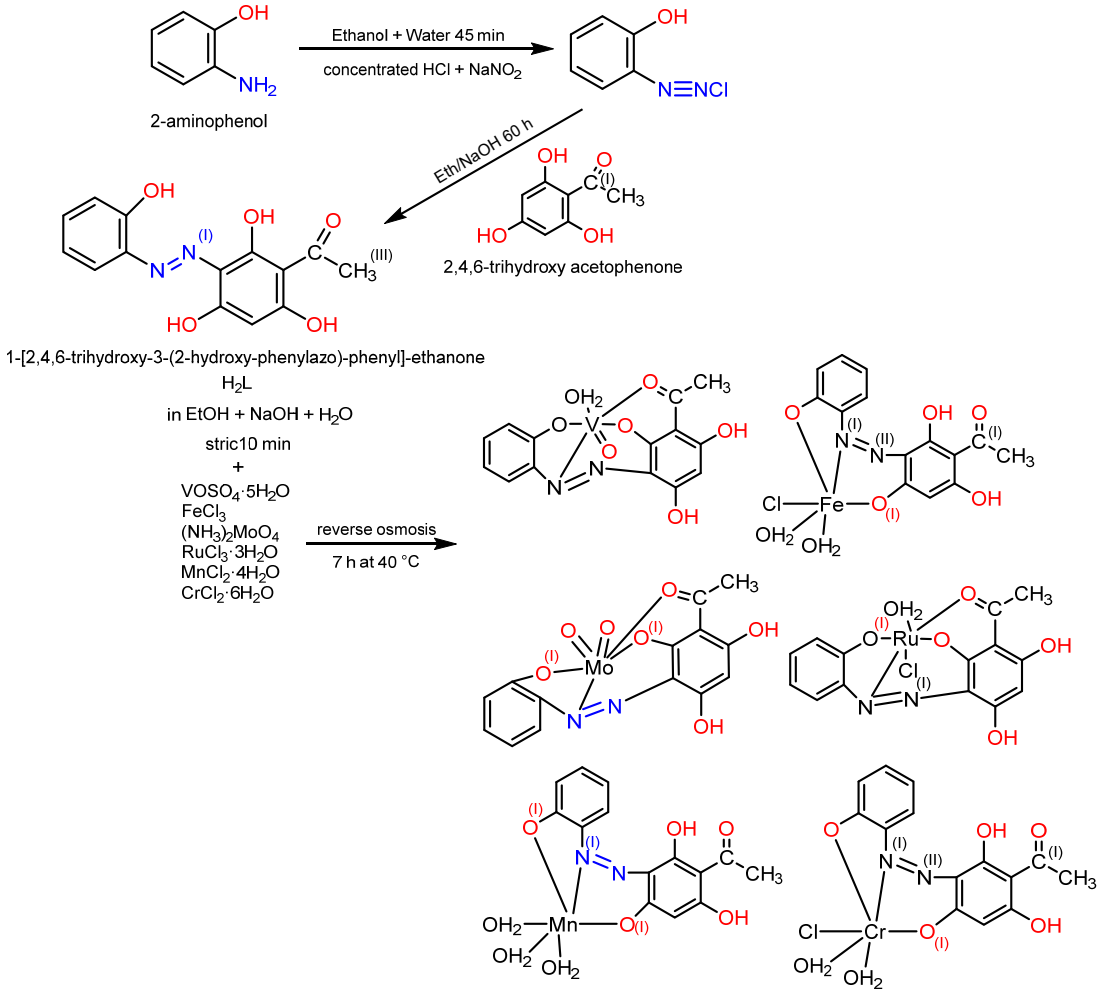

Scheme 1. Synthesis of azo dye by the diazotization-coupling reaction

growth inhibition zones around wells or disks containing the compounds, with DMSO serving as a control. The activity of the ligand and its complexes was assessed using a prepared nutrient culture medium poured into 9 cm diameter Petri dishes, which were left to solidify. A control sample without the substance was included for comparison. The dishes were then incubated upside down at a temperature of 28 ± 2 °C, and the zones of bacterial growth inhibition were measured.

Antioxidant activity

The assessment aims to determine how effectively antioxidants can neutralize free radicals. Antioxidants contribute to hydrazine, a hydrogen atom that reduces nitrogen atoms, and they also donate single electrons in 2,2-diphenyl-1-picryl-hydrazyl (DPPH). Ascorbic acid was used to evaluate and compare the antioxidant activity of metal complexes, while the DPPH test was employed to measure the scavenging of free radicals. Each antioxidant sample was diluted with an equal volume of methanol and then mixed with an identical volume of a concentrated 0.135 mM DPPH radical solution. The change in color of the hydrazine from dark violet to yellow indicates that it is undergoing radical scavenging. After adding the DPPH solution, the samples were left to stand in the dark at room temperature for 30 min. Subsequently, the absorbance of each sample was measured at 517 nm.

■ RESULTS AND DISCUSSION

Data on the ligand and complexes' physical and analytical characteristics are displayed in Table 1. According to the experimental results of the elemental analysis, every compound has a 1:1 M:L equilibrium. These data were close to the theoretically calculated values. The Cl content was calculated, yielding values close to those calculated theoretically. Furthermore, the conductivity measurements indicate that the VO-complex exhibits the highest conductivity value.

Mass Spectrometry

Mass spectrometry (MS) is a popular method for analyzing ligands and products. This technique is combined with *m/z* correlation methods to determine the molecular weight of substances [17-18]. Scheme S1 shows the mass data for the ligand and its complexes, along with the overall fragmentation pattern. The molecular ion peak appears at *m/z* = 288.94, matching the ligand's molecular weight. Additional peaks at *m/z* of 273.64, 245.23, 124.86, and 126.21 likely correspond to $C_3H_9N_2O_5^+$, $C_{12}H_9N_2O_4^+$, $C_6H_4N_2O^+$, and $C_6H_4O_3^+$

Table 1. Physical and analytical properties record for the ligand and its complexes

Compound formula M. wt (g/mol)	Color	M.p. (°C)	Yield%	Elemental microanalysis% (exp. calc.)					Conductivity in DMSO ($cm^2\ \Omega^{-1}\ mol^{-1}$)
				C	H	N	M	Cl	
$C_{14}H_{12}N_2O_5$ 288.26	Brown	192–195	78	57.97 58.33	3.79 4.19	9.88 9.71	- -	-	-
$C_{14}H_{12}N_2O_7V$ 371.20	Red	257–259	77	44.68 45.30	3.72 3.26	8.34 7.55	14.09 13.72	-	17
$C_{14}H_{16}N_2O_8Mn$ 395.22	Orange	262–264	85	43.01 42.55	4.38 4.08	7.79 7.09	14.20 13.90	-	11
$C_{14}H_{14}N_2O_7CrCl$ 409.72	Brown-light	255[d]	73	40.37 41.04	3.09 3.44	7.71 6.84	13.38 12.69	7.94 8.65	11
$C_{14}H_{14}N_2O_7FeCl$ 413.57	Yellowish-brown	230–234	81	41.08 40.66	3.68 3.41	7.69 6.77	13.08 13.50	9.43 8.57	17
$C_{14}H_{10}N_2O_7Mo$ 414.18	Brown-red	298d	88	41.21 40.60	2.02 2.43	7.69 6.76	24.01 23.16	-	9
$C_{14}H_{12}N_2O_6RuCl$ 440.78	Olive-green	279d	61	38.84 38.15	3.27 2.78	7.29 6.36	-	8.67 8.04	11

Exp: Experimental, Calc: Calculated, d means it has extended the point of breakdown

fragments, as shown in Fig. S1. The MS of the Cr-complex in Fig. S2 displays the fragmentation pattern. The molecular ion peak, representing the ligand's weight, shows several peaks at *m/z* of 409.11, 390.97, 336.67, 174.68, and 165.33, linked to different fragments: $C_{14}H_{14}CrClN_2O_7$, $C_{14}H_{11}CrClN_2O_6^+$, $C_{14}H_8CrN_2O_5^{0+}$, $C_6H_4CrNO_2^{0+}$, and $C_8H_7NO_3^+$. The Ru-complex spectra in Fig. S3 reveal its fragmentation arrangement. The molecular ion peak, indicating the ligand's weight, has peaks at *m/z* of 409.11, 390.97, 336.67, 174.68, and 165.33, corresponding to various fragments: $C_{14}H_{12}RuN_2O_6Cl$, $C_{14}H_8RuClN_2O_4^+$, $C_{13}H_8RuN_2O_4^+$, $C_7H_5NORu^+$, and $C_6H_5NO_2^+$. The Mo-complex spectra in Fig. S4 clarify the fragmentation pattern, showing the molecular ion peak with peaks at *m/z* of 440.97, 404.38, 357.67, 221.02, and 123.37, which match fragments with formulas: $C_{14}H_{10}MoN_2O_7$, $C_{14}H_8MoN_2O_5^+$, $C_{13}H_8MoN_2O_5^+$, $C_7H_5NOMo^+$, and $C_6H_5NO_2^+$. Lastly, the Mn-complex spectra in Fig. S5 display their fragmentation pattern. The molecular ion peak, reflecting the ligand's weight, features peaks at *m/z* of 395.59, 358.61, 194.99, and 165.29, associated with different fragments: $C_{14}H_6MnN_2O_8$, $C_{14}H_{11}MnN_2O_6^0$, $C_6H_6MnNO_3^+$, and $C_8H_7NO_3^+$.

^{1}H- and ^{13}C-NMR

Nuclear magnetic resonance (NMR) spectroscopy was employed to characterize the newly synthesized azo dye. The ^{1}H- and ^{13}C-NMR spectra, presented in Fig. S6 and S7, respectively, illustrate the chemical shifts observed. The ^{1}H-NMR spectrum exhibited signals at 2.41–2.51 (DMSO), 3.41 (DHO), as well as aromatic proton signals at 7.54, 7.61, 7.75, 7.93, and 8.05 ppm, and 4 hydroxyl groups resonating at 10.45, 10.50, 10.56, and 10.76 ppm [11]. The ^{13}C-NMR spectrum revealed peaks at 173.22 (C1), 170.14 (C5), 163.38 (C10), 158.26 (C8), 154.97 (C9), 149.11 (C7), 146.04 (C13), 137.64 (C12), 132.64 (C3), 127.44 (C11), 118.21 (C15), 112.97 (C14), 106.90 (C2), 103.42 (C4), 101.32 (C6), and a peak at 76.97 ppm corresponding to chloroform.

Thermal Analysis

Thermal analysis data can be provided for ligand-forming complexes. Scheme S2 displays the weight loss ratios of the ligand and its complexes, their temperature ranges, and the process by which the ligand detaches from the metal complexes. This weight loss confirms the homogeneity of the thermograms when the breakdown products and decomposition stages are analyzed [19]. It supports the findings from elemental analysis and the proposed formulas that relate the calculated values to thermal decomposition effects [20]. This work presents the thermogravimetric breakdown results of the ligand and complexes of V, Fe, Mn, and Mo at various stages. The ligand's decomposition, shown in Fig. S8, involved a single step, with a percentage decrease in its equivalent weight, $-C_{13}H_{12}N_2O_5$, of 95.837%, close to the theoretical value, despite a practical loss of 95.443%. The remaining weight (C) is theoretically 4.163%, but in practice, it's 4.557%. The DSC thermogram of the ligand was analyzed to understand its thermal behavior, as shown in Fig. S9. The decomposition of the Mn-complex, shown in Fig. S10, involved 3 stages: the first stage saw a loss of $2H_2O$, with a theoretical and practical decrease of 9.113 and 10.009%, respectively; the second stage involved losing CO_2 and H_2O, with theoretical and practical losses of 15.695 and 14.672%; and the third stage involved a loss of $C_{13}H_{10}N_2O_2$, with theoretical and practical weight reductions of 57.210 and 58.194%. The breakdown of the Mo-complex, shown in Fig. S11, included two stages: first, the loss of $2CO_2$, with theoretical and practical decreases of 21.24 and 20.864%; second, the loss of $C_{12}H_{10}N_2$, with both calculated and measured losses at 43.942%. The remaining material was MoO_3. The Fe-complex decomposition, shown in Fig. S12, involved three stages: the first stage saw an 8.704% weight loss for $2H_2O$ (theoretical) and 8.008% (practical); the second stage involved the loss of CO_2 and Cl, with theoretical and practical losses of 19.222 and 20.106%; and the third stage involved reducing $C_{13}H_{10}N_2O_2$ to 54.646% theoretically and 53.421% practically. Finally, the residual material was FeO^+. The VO-complex, shown in Fig. S13, decomposed in four stages: first, H_2O loss of 4.849% (theoretical) and 3.997% (practical); second, loss of CO_2, with 11.853% theoretically and 12.672% practically; third, loss of C_9H_8N, with 35.021% theoretically and 35.738% practically; and last, loss of $C_4H_2N_2O_2$ at 29.633% (theoretical) and 30.341% (practical). The remaining material was VO_2. Table 2

Table 2. DSC analysis of thermal decomposition for the ligand and several complexes

Compound	Step	T_i (°C)	T_f (°C)	Weight mass loss (%)		Reaction
				Estimated	Calculated	
Ligand (H_2L)	1	56.327	454.914	95.443	95.837	$-C_{13}H_{12}N_2O_5$ C
Calculated: 95.837% Final = 4.163% Estimated 95.443% Final 4.557%						
Mo-complex	1	54.257	313.429	20.864	21.246	$-C_8H_{10}N_2$-SO_4, $-2CO_2$
	2	313.429	592.714	43.942	43.942	$-C_{12}H_{10}N_2$ MoO_3
Calculated: 65.188% Final = 34.812% Estimated 64.806% Final = 35.194%						
Fe-complex	1	47.961	181.642	8.008	8.705	$-2H_2O$
	2	118.642	300.017	20.106	19.222	$-Cl$, $-CO_2$
	3	300.017	597.641	53.421	54.646	$-C_{13}H_{10}N_2O_2$ FeO^+
Calculated: 82.573% Final = 17.427% Estimated 81.535% Final = 18.465%						
VO-complex	1	53.671	170.712	3.997	4.849	$-H_2O$
	2	170.712	245.018	12.672	11.853	$-CO_2$
	3	245.018	389.163	35.738	35.021	$-C_9H_8N$
	4	389.163	591.445	30.341	29.633	$-C_4H_2N_2O_2$ VO_2
Calculated: 81.356% Final = 18.644% Estimated 82.748 % Final = 17.252%						
Mn-complex	1	56.392	170.157	10.009	9.003	$-2H_2O$
	2	170.157	264.438	14.672	15.695	$-H_2O$, $-CO_2$
	3	264.438	596.371	58.194	57.210	$-C_{13}H_{10}N_2O_2$ MnO
Calculated: 81.908 % Final = 18.092% Estimated 82.875% Final = 17.125%						

summarizes the findings of the thermal decomposition of the ligand and the thermogravimetric analysis of the complexes.

FTIR Spectrum

FTIR spectroscopy is one of the earliest and most widely used techniques for analyzing thin films produced by chemical solution deposition. This method, also known as vibrational absorption spectroscopy, provides insight into the covalent bonding within the chemical groups of the studied materials. FTIR spectroscopy can be applied to both the precursor solutions used for film deposition and the resulting thin films, regardless of the specific deposition method employed. Key insights obtained through this technique include the composition of the starting reagents, the molecular structure of mixed solutions, chemical reactions occurring during solution storage, the effect of solvent type (alcohol-based or water-based) on film properties, and the crystallization behavior of initially amorphous films during thermal treatment. The data for the ligand H_2L and its metal complexes—Fe(III), Cr(III), V(IV), Mn(II), Ru(III), and Mo(VI)—are recorded in Table 3. The ligand is shown in Fig. S14, and the complexes Ru and Mo are depicted in Fig. S15 and S16. The FTIR spectrum of the ligands exhibits moderately intense stretching bands at 3120, 2925, and 1442 cm^{-1}, which are assigned to the vibration frequencies of ν(C–H) aromatic, ν(C–O), and ν(N=N), respectively. These bands are comparable to previous research studies [21]. Additionally, the FTIR spectra of all the synthesized compounds revealed that the azo dye ligand is coordinated to the metal ions via two sites: the deprotonated oxygen of the phenol group and the nitrogen of the azo group. New bands corresponding to (M–N) are observed at (528, 596), 565, 522, 569, and 540 cm^{-1}, while M–O bands appear at 439, (449, 524), 442, (430, 520), and (432, 463) cm^{-1} for Fe-, VO-, Mn-, Ru-, and Mo-complexes, respectively.

Table 3. The locations of the distinct bands of ligand and its complexes in the infrared spectrum

Compounds	ν(C–H) aromatic	ν(C–H) aliphatic	N(C=O)	ν(N=N)	ν(O–H)	ν(M–N)	ν(M–O)	ν(H_2O) water
Ligand H_2L	3120	2925	1630	1442	3308	-	-	-
[Cr(L)(H_2O)$_2$Cl]	3131	-	1629	1400	3361			3431
[VO(L)(H_2O)]	3136	2922	1630	1402	3333	563	449 524	3425 1690 835
[Mo(L)O_2]	3141	2952	1606	1402	3307	540	432 463	-
[Mn(L)(H_2O)$_3$]	-	2960	1630	1402	3328	522	442	3444 1700 835
[Ru(L)(H_2O)Cl]	3132	2924	1601	1404	3377	569	430 520	3450 1669 828
Fe(L)(H_2O)$_2$Cl	3105	2970	1630	1401	3361	528 596	439	3485 1689 827

Electronic Spectra

UV-absorbing materials must possess several key characteristics, including high transparency, broad absorption across the UV spectrum, strong photostability, and affordability. UV absorbers are found in both inorganic and organic materials. However, the use of organic UV absorbers is severely limited due to their low stability and photo degradation under UV radiation. Metal oxide semiconductors enhance protective coatings because of their highly efficient UV absorption [22-23]. The electronic spectrum of the ligand (H_2L) shown in Table 4 exhibits significant absorption at 210 nm (47619.04 cm^{-1}), attributed to the π→π* transition, and a peak at 410 nm (24390.24 cm^{-1}), due to the n→π* transition. The electronic transitions of the VO-complex, as shown in Fig. S17 and Table 4, display peaks at 275, 325, 480, and 675 nm, corresponding to π→π*, n→π*, C.T L→M, and ^2B_2g→^2Eg transitions, which indicate a square pyramidal geometry. The Mn-complex exhibits electronic absorption peaks at 260, 300, 440, 590, and 600 nm, assigned to π→π*, C.T M→L, 6A1g→4T1g, and ^6A_1g→^4T_2g transitions, which suggest an octahedral structure. The spectrum of the Cr-complex shows peaks at 300, 340, 417, 770, and 790 nm. The ligand spectrum produces four peaks—at 250, 380, 425, 700, and 725 nm—assigned to π→π*, n→π*, C.T L→M, ^6A_1g→^4Eg (G), and ^6A_1g→^4T_2g (G), indicating an octahedral geometry. The Mo-complex exhibits peaks at 250, 420, and 590 nm, corresponding to π→π*, n→π*, and C.T L→M, indicating an octahedral shape. The spectrum of the Fe-complex, shown in Fig. S18, displays four peaks at 250, 380, 425, 700, and 725 nm, assigned to π→π*, n→π*, C.T L→M, ^6A_1g→^4Eg(G), and ^6A_1g→^4T_2g(G), confirming an octahedral structure. The Ru-complex shows peaks at 240, 275, 470, 650, and 700 nm, corresponding to π→π*, n→π*, C.T L→M, ^1A_1g→^1T_1g(G), and ^1A_1g→^1T_2g(G), indicating an octahedral geometry.

Antioxidant Activity

The complexation of carbon-based ligands with various metal ions from the d-block has been used to enhance the antioxidant performance of these ligands. Due to their numerous benefits, coordination compounds are widely utilized in industries, especially in medicine, to support and promote redox processes related to antioxidant activity. The most studied antioxidant properties of these coordination compounds involve free radical scavenging and protecting human organisms from the harmful effects of

Table 4. The UV-vis analysis of the ligand (H_2L) and its complexes

Compound	λ (nm)	ν (cm^{-1})	Abs	ε_{max} (L mol^{-1} cm^{-1})	Assignment	μ_{eff} (B.M)	Hybridization	Distribution
Ligand H_2L	210	47619.04	0.53	530	π→π*	-	-	-
	410	24390.24	1.72	1750	n→π* C.T L→L			
[VO(L)H_2O] Square pyramidal	275	36363.63	1.120	1120	π→π*	1.73	dsp^3	$t_2g^1eg^0$
	325	30769.23	0.762	762	n→π*			
	480	20833.33	0.800	800	$^2B_2g \rightarrow {}^2Eg$			
	675	14814.81	0.450	450	$^2B_2g \rightarrow {}^2B_1g$			
[Mn(L)$(H_2O)_3$] Octahedral	260	38461.53	0.600	600	π→π*	5.91	sp^3d^2	$t_2g^3eg^2$
	300	33333.33	0.560	560	C.T L→M			
	440	22727.27	0.190	190	$^6A_1g \rightarrow {}^4T_1g$			
	590	16949.15	0.145	145	$^6A_1g \rightarrow {}^4T_2g$			
	600	16666.66	0.111	111				
[Cr(L)$(H_2O)_2Cl$] Octahedral	300	33333.33	0.811	811	π→π*	3.87	d^2sp^3	$t_2g^3eg^0$
	340	29411.76	0.520	520	n→π*+C.T L→M			
	417	23980.81	1.111	1111	$^6A_1g \rightarrow {}^4Eg(G)$			
	770	12987.01	0.250	250	$^6A1g \rightarrow {}^4T_2g(G)$			
	790	12658.22	0.250	250				
[Mo(L)$O_2(H_2O)$] Octahedral	250	40000.00	2.485	2485	π→π*	diamagnetic	d^2sp^3	$t_2g^0eg^0$
	420	23809.52	1.85	185	n→π*			
	590	16949.15	0.475	475	C.T L→M			
[Fe(L)$(H_2O)_2Cl$] Octahedral	250	40000.00	1.500	1500	π→π*	5.91	sp^3d^2	$e^4t^4_2$
	380	26315.78	0.900	900	n→π*			
	425	23529.41	0.922	922	C.T L→M			
	700	14285.71	0.500	500	$^6A_1g \rightarrow {}^4Eg(G)$			
	725	13793.10	0.500	500	$^6A1g \rightarrow {}^4T_2g(G)$			
[Ru(L)$(H_2O)Cl$] Octahedral	240	41666.66	1.550	1550	π→π*	1.73	d^2sp^3	$t_2g^5eg^0$
	275	36363.63	0.900	900	n→π*			
	470	21276.59	0.550	550	C.T L→M			
	650	15384.61	0.250	250	$^1A_1g \rightarrow {}^1T_1g(G)$			
	700	14285.71	0.250	250	$^1A1g \rightarrow {}^4T_1g(G)$			

free radicals. Colorimetric techniques are the most common methods; however, electron paramagnetic resonance (EPR) is an alternative for metallic compounds, as color does not influence the results [24]. The antioxidant activity of H_2L and its metal complexes was examined with ascorbic acid, and free radicals were scavenged using the DPPH assay. Each sample was first diluted with the same volume of methanol and then combined with the same volume of a 0.135 mM DPPH solution after addition [25-26]. The complex with a lower IC_{50} value has a stronger ability to inhibit free radicals than ascorbic acid. The ligand exhibits the highest free radical inhibition activity, followed by the Ru-complex, then the Fe-complex, ascorbic acid, the VO-complex, and the Mo-complex, all of which have an IC_{50} of 0.229 μg/mL. The Mn-complex is next, followed by the Cr-complex, which is the least effective. From Table 5, it can be concluded that metal ions may sometimes act as pro-oxidants (depending on the metal's characteristics, concentration, the specific antioxidant structure, and environmental conditions), leading to oxidative damage by generating free radicals instead of neutralizing them. Thus, adding metals does not always increase antioxidant activity. Furthermore, complex formation that destabilizes electron density and diminishes antioxidant capacity can result from adverse interactions

Table 5. The antioxidant results of H_2L and its complexes

Compound	Concentration (μg/mL)	PI%	RSA%	IC_{50} (μg/mL)
Ascorbic acid	0.128	17.779	82.221	0.229
	0.064	29.027	70.027	
	0.032	43.458	56.542	
	0.016	50.757	49.243	
	0.008	54.158	45.842	
Ligand	0.128	15.430	84.570	0.221
	0.064	29.960	70.040	
	0.032	40.560	59.440	
	0.016	47.330	52.670	
	0.008	50.410	49.590	
Fe-complex	0.128	22.353	77.647	0.224
	0.064	27.053	72.947	
	0.032	31.328	68.672	
	0.016	33.053	66.947	
	0.008	37.326	62.674	
Ru-complex	0.128	16.127	83.873	0.222
	0.064	23.186	76.814	
	0.032	28.624	71.376	
	0.016	33.082	66.918	
	0.008	38.625	61.375	
Mo-complex	0.128	11.625	88.375	0.229
	0.064	18.429	81.571	
	0.032	22.606	77.394	
	0.016	25.629	74.371	
	0.008	30.186	69.814	
VO-complex	0.128	26.059	73.941	0.229
	0.064	37.053	62.947	
	0.032	44.328	55.672	
	0.016	51.766	48.234	
	0.008	55.913	44.087	
Cr-complex	0.128	17.530	80.370	0.235
	0.064	31.340	71.660	
	0.032	39.420	67.580	
	0.016	41.320	60.350	
	0.008	43.110	56.220	
Mn-complex	0.128	11.059	88.941	0.234
	0.064	28.049	71.951	
	0.032	42.269	57.731	
	0.016	51.766	48.234	
	0.008	57.768	42.232	

with the ligand or from unsuitable oxidation states, redox potentials, or charge distributions (see Fig. S19–S26).

Biological Activity

Bacteria

The broth dilution method was used to test the antibacterial properties of the currently synthesized azo dye ligand and its complexes against *Bacillus* spp. and *E. coli* [27]. Transition metal ions have contributed to a diverse and rich field of research, garnering much attention due to their applications in biology, medicine, and industry. Coordination compounds of azo dyes have garnered interest due to their ability to mimic complex molecules involved in vital biological processes [28-29], such as oxygen transport, electron transfer, and catalysis [30-32].

The biological activity of the targets against *E. coli* and *Bacillus* spp. is as follows: The ligand shows an apparent effect against *E. coli* and *Bacillus* spp., as shown in Fig. S27. Its activity decreased as the concentration increased from 1 to 500 (from 17 to 14 against *E. coli* and from 26 to 19 against *Bacillus* spp.). The complexes exhibit different activities at the two concentrations (1 and 500). The Mn-complex has greater activity against *Bacillus* spp. at 500 concentration, but the Fe-complex shows greater activity against *E. coli*, as presented in Fig. S28 and S29, respectively. The VO-complex exhibits no activity, as displayed in Fig. S30, against *E. coli* and *Bacillus* spp. Fig. S31 and S32, as well as Table 6, show the complete details.

Fungi

From Table 6 and Fig. S33, the biological activity of the ligand and its complexes against fungi (*Penicillium, Aspergillus*, *Fusarium*, and *Trichoderma*) is evident. The ligand showed minimal biological activity against the fungi, while higher activity against *Penicillium* was observed with the Fe-complex and Mo-complex (8) at a concentration of 500. The highest activity against *Aspergillus* was observed with the VO-complex (25) at a concentration of 500. The highest activity against *Fusarium* was with Mo-complex (17) at a concentration of 500, and the highest activity against *Trichoderma* was with Ru-complex (21) at a concentration of 1. Overall, some complexes had selective effects on specific fungal species, suggesting they could serve as antifungal agents

Table 6. Biological activity of ligand and its complexes against fungi and bacteria

Complexes	Conc. (M)	*Penicillium* (mm)	*Aspglisniger* (mm)	*Fusarum* (mm)	*Trichoerma* (mm)	*E. coli* (mm)	*Bacillus* spp. (mm)
Control (DMSO)		10	30	20	50		
Ligand	1	2	1	2	5	17	26
	500	1	1	3	3	14	19
Fe-complex	1	6	1	16	12	22	-
	500	8	10	15	15	10	8
Mn-complex	1	5	11	6	18	10	10
	500	5	12	12	20	12	28
VO-complex	1	6	16	15	5	-	-
	500	6	25	15	15	-	-
Ru-complex	1	6	12	12	21	14	4
	500	7	12	15	20	10	12
Mo-complex	1	4	12	13	10	8	4
	500	8	13	17	18	14	8

depending on the target fungus [30]. The increased activity of the complexes can be explained by Tweedy's chelation theory [33].

■ CONCLUSION

In conclusion, using a simple replacement procedure involving 2,4,6-trihydroxyacetophenone, we successfully produced a new azo dye ligand derivative (H_2L) with 2-aminophenol. Then, the assembly of this ligand with salts of V(IV), Fe(III), Cr(III), Mn(II), Mo(VI), and Ru(III) was achieved satisfactorily. The ligand acted as a tri and tetradentate chelate, while the resulting complexes have the general formula $[M(L)X_n]$ where X = H_2O, M = VO, MoO_2, Mn (n = 1, 1, and 3, respectively), or X = H_2O and Cl, M = Cr, Fe (n = $2H_2O$ and 1Cl), Ru (n = $1H_2O$ and 1Cl). All complexes were non-electrolytic and exhibited various octahedral geometries, except for the vanadium complex, which had a square pyramidal structure. After calculating the IC_{50} values, it was shown that the ligand has a strong capacity to inhibit free radicals. (H_2L > Ru-complex > Fe-complex > ascorbic acid = VO-complex = Mo-complex > Mn-complex > Cr-complex). These complexes could thus act as inhibitors of free radicals. Additionally, the complexes were tested at two different doses for their antifungal and antibacterial properties against four different fungi and two bacterial species.

■ ACKNOWLEDGMENTS

The authors express their gratitude to the staff of the Chemistry Department at the University of Baghdad, College of Science for Women, for their support and encouragement.

■ CONFLICT OF INTEREST

The authors have no conflict of interest.

■ AUTHOR CONTRIBUTIONS

Ban Hasan Ali Al-Agele: Data duration, Analysis, Funding achievement, Investigation, Methodology, Writing—original draft. Areej Kamal Assim Al-Dabbagh: Conceptualization, Data duration, Recognized analysis, Investigation, Methodology, Project administration, Supervision, Writing—review and editing. Both authors have read and approved the manuscript.

■ REFERENCES

[1] Riaz, N.N., Iqbal, S., Amin, S., Ahmad, K., Atif, M., Muhammad, S., Ahmed, M.M., and Ashfaq, M., 2025, Rational synthesis of azo ligands and copper complexes: Insights into potential therapeutic agents, *J. Mol. Struct.*, 1321, 139705.

[2] Al-naemi, A.A.A., and Al-Hamdani, A.A.S., 2025, Synthesis and characterization of new azo dye

complexes and studies of antioxidant, bioactivity and thermal analysis, *Bull. Chem. Soc. Ethiop.*, 39 (8), 1559–1578.

[3] Al-Rubaye, N.T.A., and Al-Hamdani, A.A.S., 2025, Synthesizing and characterization of some metal ion complexes with new azo dye and studying antioxidant and anticancer (MCF-7), *Bull. Chem. Soc. Ethiop.*, 39 (5), 859–875.

[4] Mohammed, H.S., 2020, Synthesis, characterization, structure determination from powder X-ray diffraction data, and biological activity of azo dye of 3-aminopyridine and its complexes of Ni(II) and Cu(II), *Bull. Chem. Soc. Ethiop.*, 34 (3), 523–532.

[5] Abd El-Lateef, H.M., Khalaf, M.M., Amer, A.A., Kandeel, M., Abdelhamid, A.A., and Abdou, A., 2023, Synthesis, characterization, antimicrobial, density functional theory, and molecular docking studies of novel Mn(II), Fe(III), and Cr(III) complexes incorporating 4-(2-hydroxyphenyl azo)-1-naphthol (Az), *ACS Omega*, 8 (29), 25877–25891.

[6] Al-Qahtani, S.D., Alnoman, R.B., Alatawi, N.M., Alkhamis, K.M., Bayazeed, A., Alsoliemy, A., and El-Metwaly, N.M., 2023, Improvement of dye-sensitized solar cells' performance via co-sensitization of new azo thiazole organic dyes with ruthenium(II) based N-719 dye, *J. Saudi Chem. Soc.*, 27 (3), 101643.

[7] El-Wakiel, N., 2018, Nano-sized metal complexes of azo L-histidine: Synthesis, characterization and their application for catalytic oxidation of 2-amino phenol, *Appl. Organomet. Chem.*, 32 (4), e4229.

[8] Rezaei-Seresht, E., Salimi, A., and Mahdavi, B., 2019, Synthesis, antioxidant and antibacterial activity of azo dye-stilbene hybrid compounds, *Pigm. Resin Technol.*, 48 (1), 84–88.

[9] Bhowmik, S., Sengupta, A., and Mukherjee, R., 2024, Ni(II) and Pd(II) complexes of a new redox-active pentadentate azo-appended 2-aminophenol ligand: Pd(II)-assisted intraligand cyclization forms a phenoxazinyl ring, *Dalton Trans.*, 53 (33), 14046–14064.

[10] Liu, S.H., Cao, C.R., Lin, W.C., and Shu, C.M., 2019, Experimental and numerical simulation study of the thermal hazards of four azo compounds, *J. Hazard. Mater.*, 365, 164–177.

[11] Hung, L.C., and Pan, N.H., 2023, Using thermal analysis with kinetic calculation method to assess the thermal stability of azo compound on construction materials, *J. Loss Prev. Process Ind.*, 84, 105107.

[12] Fadhel, A.M., Al-Hamdani, A.A.S., and Al Zoubi, W., 2025, Synthesis, characterization, and thermal studying of VO(II), Cu(II), Zn(II), Cd(II), and Au(III) complexes with azo dye and evaluation as antioxidants, *Baghdad Sci. J.,* 22 (1), 86–102.

[13] Khanum, R., Shoukat Ali, R.A., Rangaswamy, H.R., Santhosh Kumar, S.R., Prashantha, A.G., and Jagadisha, A.S., 2023, Recent review on Synthesis, spectral Studies, versatile applications of azo dyes and its metal complexes, *Results Chem.*, 5, 100890.

[14] Mahmoud, W.H., Sayed, F.N., and Mohamed, G.G., 2016, Synthesis, characterization and *in vitro* antimicrobial and anti-breast cancer activity studies of metal complexes of novel pentadentate azo dye ligand, *Appl. Organomet. Chem.*, 30 (11), 959–973.

[15] Venugopal, N., Krishnamurthy, G., Bhojyanaik, H.S., and Giridhar, M., 2019, Novel bioactive azo-azomethine based Cu(II), Co(II), and Ni(II) complexes, structural determination and biological activity, *J. Mol. Struct.,* 1191, 85–94.

[16] Abdulridha, M.Q., Al-Hamdani, A.A.S., and Al Zoubi, W., 2023, Synthesis, spectral identification, thermal and antioxidant studies for Ni(II), Pd(II), Pt(IV) and Au(III) complexes with new azo ligand derivatives from tryptamine, *Ibn AL-Haitham J. Pure Appl. Sci.*, 36 (4), 303–320.

[17] Al-Daffay, R.K.H., and Al-Hamdani, A.A.S., 2023, Synthesis, characterization, and thermal analysis of a new acidicazo ligand's metal complexes, *Baghdad Sci. J.*, 20 (1), 121–133.

[18] Hamza, I.S., Mahmmoud, W.A., Al-Hamdani, A.A., Ahmed, S.D., Allaf, A.W., and Al Zoubi, W., 2022, Synthesis, characterization, and bioactivity of several metal complexes of (4-amino-*N*-(5-methyl-isaxazol-3-yl)-benzenesulfonamide), *Inorg. Chem. Commun.*, 144, 109776.

[19] Masoud, M.S., Hemdan, S.S., and Elsamra, R.M.I., 2023, Synthesis, ligating properties, thermal behavior, computational and biological studies of some azo-transition metal complexes, *J. Inorg. Organomet. Polym. Mater.*, 33 (1), 120–137.

[20] Nguyen, T.L., and Saleh, M.A., 2020, Thermal degradation of azobenzene dyes, *Results Chem.*, 2, 100085.

[21] Cinar, M., Coruh, A., and Karabacak, M., 2014, A comparative study of selected disperse azo dye derivatives based on spectroscopic (FT-IR, NMR and UV–vis) and nonlinear optical behaviors, *Spectrochim. Acta, Part A*, 122, 682–689.

[22] Pinheiro, H.M., Touraud, E., and Thomas, O., 2004, Aromatic amines from azo dye reduction: Status review with emphasis on direct UV spectrophotometric detection in textile industry wastewaters, *Dyes Pigm.*, 61 (2), 121–139.

[23] Cardito, A., Carotenuto, M., Sacco, O., Albarano, L., Vaiano, V., Iannece, P., Libralato, G., Spica, V.R., and Lofrano, G., 2024, UV light assisted degradation of acid orange azo dye by ZVI-ZnS and effluent toxicity effects, *Environ. Pollut.*, 343, 123226.

[24] Sarvalkar, P.D., Jamadar, A.S., Kakade, S.S., Magdum, A.B., Pawar, P.K., Yadav, J.B., Nimbalkar, M.S., Prasad, N.R., Ramteke, A.A., and Sharma, K.K.K., 2024, Biogenic synthesis of Co_3O_4 nanoparticles from *Aloe barbadensis* extract: Antioxidant and antimicrobial activities, and photocatalytic degradation of azo dyes, *Results Eng.*, 22, 102094.

[25] Al-Adilee, K.J., Jawad, S.H., Kyhoiesh, H.A.K., and Hassan, H.M., 2024, Synthesis, characterization, biological applications, and molecular docking studies of some transition metal complexes with azo dye ligand derived from 5-methyl imidazole, *J. Mol. Struct.*, 1295, 136695.

[26] Abd El-Lateef, H.M., El-Dabea, T., Khalaf, M.M., and Abu-Dief, A.M., 2023, Recent overview of potent antioxidant activity of coordination compounds, *Antioxidants*, 12 (2), 213.

[27] Ghanbari, H., Derakhshankhah, H., Bahrami, K., Keshavarzi, S., Mohammadi, K., Hayati, P., Centore, R., and Parisi, E., 2024, Synthesis, characterization, and biological activity of a fresh class of sonochemically synthesized Cu^{2+} complexes, *Sci. Rep.*, 14 (1), 21325.

[28] Saleh, M.G., El-Sayed, W.A., Zayed, E.M., Shawky, M., and Mohamed, G.G., 2024, Analyzing the structure of the metal complexes of biologically active azo dye ligand, *Appl. Organomet. Chem.*, 38 (4), e7397.

[29] Mahmood Taher, A., Ali Kadhim Kyhoiesh, H., Shakir Waheeb, A., Al-Adilee, K.J., and Jasim, L.S., 2024, Synthesis, characterization, biological activity, and modelling protein docking of divalent, trivalent, and tetravalent metal ion complexes of new azo dye ligand (N,N,O) derived from benzimidazole, *Results Chem.*, 12, 101911.

[30] Mohammed, Z.H., and Jawad, S.A.A., 2025, Preparation, diagnosis and studying the biological activity of multi dentate azo-Schiff ligand and some of its complexes, *Morrocan J. Chem.*, 13 (3), 1196–1209.

[31] Jarrahpour, A.A., Motamedifar, M., Pakshir, K., Hadi, N., and Zarei, M., 2004, Synthesis of novel azo Schiff bases and their antibacterial and antifungal activities, *Molecules*, 9 (10), 815–824.

[32] Khalaf, M.M., Abd El-Lateef, H.M., Gouda, M., Abdelhamid, A.A., Amer, A.A., and Abdou, A., 2024, Designing, characterization, DFT, biological effectiveness, and molecular docking analysis of novel Fe(III), Co(II), and Cu(II) complexes based on 4-hydroxy-2*H*-pyrano[3,2-c]quinoline-2,5(6*H*)-dione, *ACS Omega*, 9 (6), 6466–6481.

[33] Bongoza, U., Zamisa, S.J., Munzeiwa, W.A., and Omondi, B., 2022, Silver(I) complexes of *N*,*N*′-diarylformamidine ligands: Synthesis, crystal structures, and *in vitro* antibacterial studies, *Appl. Organomet. Chem.*, 36 (7), e6726.